Building Characterization Using L-Band Polarimetric Interferometric SAR Data

Stéphane Guillaso, *Member, IEEE*, Laurent Ferro-Famil, *Member, IEEE*, Andreas Reigber, *Member, IEEE*, and Eric Pottier, *Member, IEEE*

***Abstract*—This letter proposes a building characterization technique for L-band polarimetric interferometric synthetic aperture radar (SAR) data. This characterization consists of building identification and height estimation. Initially, a polarimetric interferometric segmentation is performed to isolate buildings from their surroundings. This classification identifies three basic categories: single bounce, double bounce, and volume diffusion. In order to compensate for the misclassifications among the volume and the double-bounce classes, interferometric phases given by the high-resolution Estimation of Signal Parameters via Rotational Invariance Techniques (ESPRIT) method are analyzed. Once buildings are localized, a phase-to-height procedure is applied to retrieve building height information. The method is validated using E-SAR, German Aerospace Center (DLR) fully polarimetric SAR data, at L-band, repeat-pass mode, over the Oberpfaffenhofen, Germany, test site, with a spatial resolution of 1.5 m in range and azimuth. More than 80% of buildings are retrieved with acceptably accurate height estimates.**

***Index Terms*—Building characterization, classification, Estimation of Signal Parameters via Rotational Invariance Techniques (ESPRIT), interferometry, polarimetry.**

I. Introduction

ONE of the main applications in urban remote sensing is the analysis of buildings. This process consists of, first, the differentiation of buildings and surroundings, and, second, the characterization of located buildings. Building characterization consists of retrieving all relevant parameters concerning a building: shape (length, width) and height. In the scope of this study, the characterization of buildings is reduced to the estimation of their height.

The purpose of this letter is to propose a polarimetric interferometric method to localize and characterize buildings, using L-band synthetic aperture radar (SAR) data, by linking the physical nature of a scatterer with its spatial geometry [1]. This approach consists of three stages. The building localization is performed using a polarimetric and polarimetric interferometric segmentation. The polarimetric segmentation is based on an unsupervised Wishart H-A-α classification scheme. An interpretation is attached to the resulting clusters using parameters obtained from the eigendecomposition of a sample coherency matrix, and the observed scene is classified to identity three general types of scattering mechanism: single bounce, double bounce, and volume. Due to the overlap of the volume and double-bounce classes, an additional classification based on a polarimetric/interferometric technique is applied to the volume class. Optimal coherences, introduced in [2], are used as an input to the Wishart probability distribution of polarimetric interferometric coherency matrices. These approaches are presented in Sections II-A and B. In order to compensate for misclassifications in the building class, an analysis of the interferometric phase, given by the high-resolution Estimation of Signal Parameters via Rotational Invariance Techniques (ESPRIT) method, is proposed in Section II-C. Using these interferometric phases, a phase-to-height procedure is applied over building locations to retrieve building heights. This is presented in Section II-D. Section III contains conclusions regarding this work.

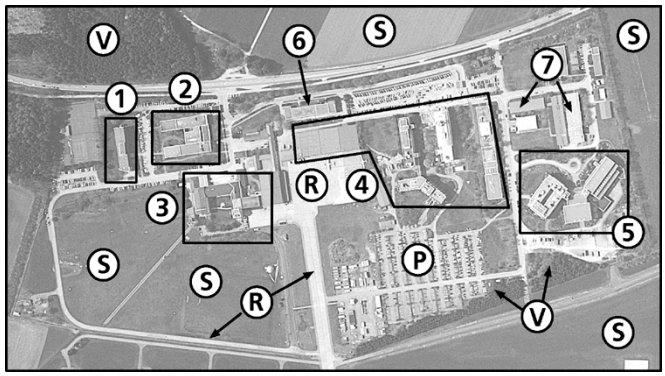

Fig. 1. Aerial photograph of the DLR test site. Numbers (1)–(7) indicate the locations of the buildings under study. The other media present in the scene are (R) roads, (V) forests, (S) fields, and (P) parking lot.

The proposed method is validated using polarimetric interferometric SAR data acquired over the Oberpfaffenhofen test site. These data were acquired in L-band (0.23-m wavelength) repeat-pass mode by the German Aerospace Center (DLR) E-SAR system. The spatial resolution of the data used is 1.5 m in range and azimuth. The interferometric baseline used is about 6.0 m. The scene under study is the DLR site, which has some isolated buildings surrounded by complex media like green fields, roads, and forests. Fig. 1 shows an aerial photograph of the chosen test site. Numbers (1)–(7) indicate the locations of the buildings under study. The other media present in the scene are roads (R), forests (V), fields (S), and a parking lot (P).

Manuscript received November 13, 2004; revised February 23, 2005. This work was supported in part by the German Science Foundation DFG under Project RE 1698/1.

S. Guillaso and A. Reigber are with the Department of Computer Vision and Remote Sensing, Berlin University of Technology, D-10587 Berlin, Germany (e-mail: stephane@cs.tu-berlin.de; anderl@cs.tu-berlin.de).

L. Ferro-Famil and E. Pottier are with the University of Rennes 1, Institut of Electronic and Telecommunication of Rennes, F-35042 Rennes, France (e-mail: laurent.ferro-famil@univ-rennes1.fr; eric.pottier@univ-rennes1.fr).

Digital Object Identifier 10.1109/LGRS.2005.851543

II. Building Detection and Characterization

A. Polarimetric Classification

The polarimetric classification is performed in the following two steps.

Step 1) Unsupervised Wishart H-A-α segmentation: This classification is based on the coherency matrix $[T]$ derived from the scattering vector $\vec{k}$

$$[T] = \langle \vec{k}^{\dagger} \vec{k} \rangle$$

with

$$\vec{k} = \frac{1}{\sqrt{2}} [S_{HH} + S_{VV}, S_{HH} - S_{VV}, 2S_{HV}]^T. \qquad (1)$$

Over homogeneous areas, the n-look coherency matrix $[T]$ follows the complex non- probability density function $W_c(n, [\Sigma_T])$. Based on this fact, a maximum-likelihood (ML) classifier has been developed [3], which assigns each pixel in the SAR image to the class X_m to minimize the distance

$$\mathrm{d}\left([T], X_m\right) = \ln |[\Sigma_m]| + \mathrm{tr}\left([\Sigma_m]^{-1}[T]\right) \qquad (2)$$

where $[\Sigma_m]$ is the mean covariance matrix of pixels in class X_m.

The unsupervised Wishart H-A-α segmentation scheme consists of an iterative k-means clustering procedure using the ML distance defined in (2). The initialization of the class centers in the space of coherency matrices is based on the polarimetric indicators: H (entropy), A (anisotropy), and α, derived from an eigendecomposition of the sample coherency matrix $[T]$ [4], [5].

Step 2) Segmented dataset characterization: The categorization into the basic types of scattering mechanisms is given by an interpretation of the polarimetric indicators. H, the entropy, indicates the random aspect of the global scattering phenomenon; A, the anisotropy, reflects the relative importance of the two secondary scattering mechanisms; and α indicates the nature of the scattering mechanisms. α varies from 0°, corresponding to an isotropic surface, to 90°, indicating an isotropic dihedral or helix [6]. This characterization gives the principal physical nature of scattering mechanism for each Wishart class. Then, three main classes are obtained: double-bounce scatterer, which indicates the presence of buildings, single bounce, in the case of surface areas, and volume diffusion for vegetation or forest.

Each cluster obtained from the Wishart H-A-α segmentation procedure is characterized according to its most representative eigenvalue spectrum, evaluated in the H-A plane as follows [7]:

- —*Low entropy or medium entropy and low anisotropy: one dominant scatterer.* Single- and double-bounce scatterings are separated by $\alpha_1 < 45°$ and $\alpha_1 > 45°$. α_1 is calculated from the eigenvector corresponding to the largest eigenvalue.
- —*Medium entropy and high anisotropy: two significant mechanisms.* A distributed coherency matrix $\langle [T] \rangle$ is constructed from the first two elements of the eigenvector expansion. The nature of the scattering is determined from the first two Huynen generators $2A_0$ and $B_0 + B$ [8].
- —*High entropy: three significant mechanisms.* Random polarimetric scattering is associated with volume diffusion.

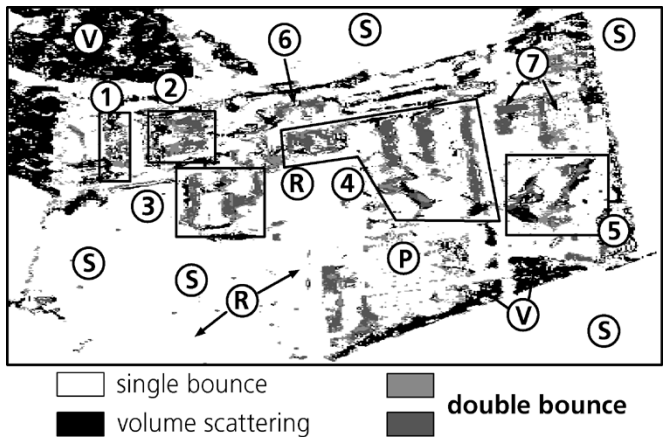

Fig. 2. Polarimetric dataset segmented using the unsupervised Wishart H-A-α classification. Three main classes are identified: single bounce (surface), double bounce (building), and volume scattering (vegetation). Misclassified pixels can be observed, especially for building group (5), due to the overlap of the volume and double-bounce classes.

The unsupervised Wishart segmentation with data characterization is applied to the Oberpfaffenhofen test site, presented in Section I. Results are shown in Fig. 2. This classification is a good description of the test site, and the major types of natural media are well defined (Figs. 1 and 2). Vegetation areas (V) and surfaces (R), (S) are accurately identified. Buildings are, to a large extent, detected well, but some misclassification between the volume class and the double class is evident [groups (4) and (5) in Fig. 2]. This is mostly due to the orientation of the building relative to the radar line of sight.

In order to improve the accuracy of building detection, further information has to be used. An analysis of the interferometric coherence can be useful to distinguish buildings from vegetation.

B. Polarimetric Interferometric Classification

The polarimetric interferometric coherent information may be represented by a (6 × 6) coherency matrix $[T_6]$ as follows:

$$[T_6] = \langle \vec{k} \vec{k}^{\dagger} \rangle = \begin{bmatrix} [T_1] & [\Omega_{12}] \\ [\Omega_{12}]^{\dagger} & [T_2] \end{bmatrix} \text{ with } \vec{k} = \begin{bmatrix} \vec{k}_1 \\ \vec{k}_2 \end{bmatrix} \qquad (3)$$

where $\vec{k}_1$ and $\vec{k}_2$ represent the target vectors from separate images and $[\Omega_{12}]$ corresponds to the (3 × 3) interferometric cross-correlation matrix.

The coherence between the different channels is, in addition to the polarimetric information, an important indicator for the properties of the underlying scattering mechanism.

In [2], a coherence optimization procedure is developed to obtain an optimal set of coherences $\{\gamma_{\mathrm{opt}_1}, \gamma_{\mathrm{opt}_2}, \gamma_{\mathrm{opt}_3}\}$ representing the square root of the eigenvalues of the non-Hermitian matrices [2. eq. (28)]. The set of optimal coherences characterizes a scene and is independent of the radar polarimetric measurement basis. The value of the coherence is maximized in each channel by projecting the target vector onto a specific scattering vector.

The optimal coherences exhibit an enhanced contrast and constitute highly descriptive indicators that can be used effectively in a classification process.

—Areas where the three optimized coherences are similar and independent of the polarization. Such behavior is characteristic of point scatterers and bare soils.
—Areas where only one optimized coherence is dominant indicate the presence of a single dominant coherent mechanism within the resolution cell. In this case secondary coherences are significantly lower. This corresponds mostly to surfaces with low SNR responses and certain fields.
—Forested areas are characterized by a single dominant mechanism, but have a very low coherence.

Rules to segment optimized coherences, proposed in [7], introduce new characteristic indicators A_1 and A_2 describing the distribution of the optimized coherences in different channels

$$A_1 = \frac{\left|\gamma_{\text{opt}_1}\right| - \left|\gamma_{\text{opt}_2}\right|}{\left|\gamma_{\text{opt}_1}\right|} \quad A_2 = \frac{\left|\gamma_{\text{opt}_1}\right| - \left|\gamma_{\text{opt}_3}\right|}{\left|\gamma_{\text{opt}_1}\right|}. \quad (4)$$

These parameters give the relative variation amplitude of the different optimized channels. As in the polarimetric case, the indicators A_1 and A_2 may be used to estimate the number of independent coherent scattering mechanisms in a resolution cell. A value for A_1 close to 1 indicates a single coherent scattering mechanism in the resolution cell, while A_1 and A_2 simultaneously close to 0 suggests weak dependence of the scattering coherence to the polarization. This information may be combined with the results of the polarimetric classification presented in Section II-A in order to classify the areas corresponding to one of the three canonical scattering mechanisms. An unsupervised Wishart classification, initialized with the results of the optimal coherence spectrum segmentation, is applied to interferometric coherency matrices contained in the volume scattering areas.

The inclusion of interferometric information helps to correct the misclassifications obtained in the polarimetric classification: vegetation areas are characterized by high volume (and temporal) decorrelation, whereas buildings are very stable in terms of interferometric coherence. Using this polarimetric interferometric classification approach, a refined double-bounce class may be estimated. Using this double-bounce class, an improved building mask can be obtained, as shown in Fig. 4. In this mask, all building groups are well detected, but some vegetation areas are still classified as buildings. This is especially the case for the vegetated areas indicated by (V) in Figs. 1 and 4. This is due to the baseline dependency of the interferometric coherence. In this application, the chosen baseline is relatively small (around 6.0 m), and some vegetated parts do not exhibit significant baseline decorrelation.

In conclusion, polarimetric and a polarimetric interferometric classification are necessary, but not sufficient for the localization of buildings. The use of the interferometric phase information as an additional parameter is required.

C. Interferometric Phase Estimation

In the case of SAR data, backscattered waves result from the sum of different scattering mechanisms. The interferometric phase obtained depends strongly on the medium under observation. Interferometric phases can be estimated using a high-resolution algorithm like ESPRIT, often employed for direction-of-arrival (DoA) estimation in the case of antenna arrays [9]. The main idea of the high-resolution method is to separate the signal from noise. This approach was initially introduced in SAR analysis [10] to study forested areas, where a SAR signal model adapted to ESPRIT algorithm was proposed.

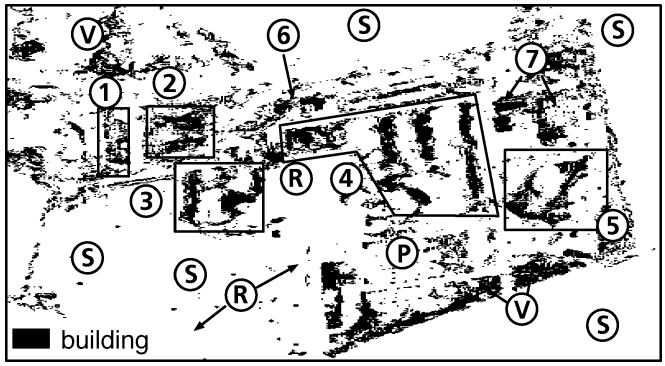

Fig. 3. Initial mask of building locations. This mask is obtained after applying a polarimetric interferometric segmentation and corresponds to the double-bounce class. The building location is overestimated, and some vegetation areas (V) are also detected as building.

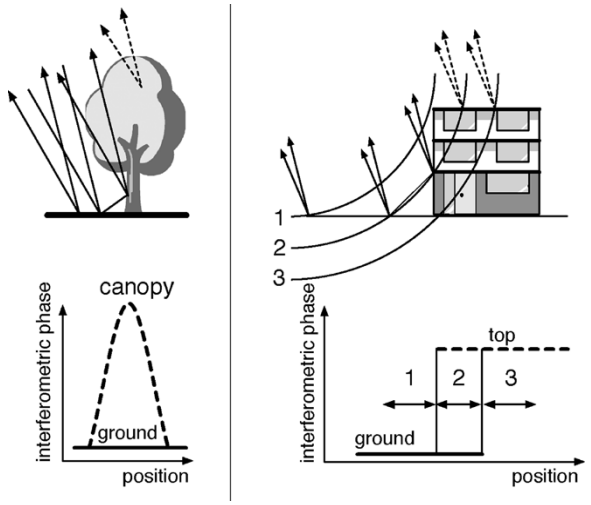

Fig. 4. ESPRIT interferometric phase behavior over different media. (Left) Optimized phases over a tree. The two phases correspond to the ground or ground–trunk and canopy reflection. This value difference is very high. (Right) Optimized phases over a building. The two phases correspond to the ground or ground–wall and top reflection.

Signals acquired during an interferometric measurement, s_1 and s_2, can be written as

$$s_1^{pq} = \sum_{m=1}^{d} \sigma_m \zeta_m^{pq} \mathrm{e}^{i\frac{4\pi}{\lambda}R} + n_1^{pq}$$
$$s_2^{pq} = \sum_{m=1}^{d} \sigma'_m \zeta_m'^{pq} \mathrm{e}^{i\frac{4\pi}{\lambda}(R+\Delta R_m)} + n_2^{pq} \quad (5)$$

where pq denotes the polarization channel (HH, HV, VH or VV). These signals consist of a sum of d different elementary scattering contributions: ζ_m^{pq} and $\zeta_m'^{pq}$ denote the normalized backscattering coefficients of the mth local scatterer in the pq polarization, and σ_m and σ'_m denote the intensity of the mth local scatterer. R is the slant range distance between scatterer and the master orbit. ΔR_m is the range difference between

master and slave tracks for the mth scatterer. Finally, n_m^{pq} denotes additive Gaussian noise in the pq polarization channel. Using a matrix and vector notation, (5) may be written as

$$\vec{s}_1 = [A]\vec{\sigma} + \vec{n}_1 \quad \vec{s}_2 = [A']\vec{\sigma}' + \vec{n}_2$$

with

$$\vec{s}_{1,2} = \left[s_{1,2}^{HH}, s_{1,2}^{HV}, s_{1,2}^{VH}, s_{1,2}^{VV}\right]^T. \tag{6}$$

Since the targets are located in the far-field region, scattering coefficients of each local scatterer are assumed to be remain identical in both interferometric acquisitions: $\zeta_m^{pq} = \zeta_m'^{pq}, \sigma_m = \sigma_m'$. Then, $\vec{s}_2$ may be simplified as follows:

$$\vec{s}_2 = [A][\Phi]\vec{\sigma} + \vec{n}_2 \text{ with } [\Phi] = \mathrm{diag}\{\mathrm{e}^{i\phi_1}, \mathrm{e}^{i\phi_2}, \cdots, \mathrm{e}^{i\phi_d}\}. \tag{7}$$

The form of (6) and (7) is adapted to the ESPRIT algorithm, and the interferometric phase of each dominant scatterer, given by $[\Phi]$, can be estimated by this method [9].

It has been shown that interferometric phases provided by the ESPRIT algorithm make it possible to remove the vegetation phase bias [11], [12]. Indeed, the ESPRIT algorithm allows one to retrieve a number of phases depending on the number of dominant scattering mechanisms present in the resolution cell. This means that the phase behavior may differ, depending on the observed medium (Fig. 4).

Over vegetated areas, two interferometric phases, corresponding to ground or ground–trunk and canopy reflection, are retrieved. In Fig. 4 (left), the behavior of the interferometric phase generated by the ESPRIT algorithm over a tree is shown. The dashed curve corresponds to the phase of the canopy reflection, while the solid curve corresponds to ground or ground–truck reflection. Over a building, the interferometric phase behavior is different (Fig. 4, right). Three cases can be distinguished. The first case corresponds to the wave reflecting before it reaches the building. Only the ground reflection is present. The second case is the most crucial: in this case, the wave reaches the building and multiple reflections need to been detected. The ESPRIT algorithm is employed to find the phase corresponding to the ground and the ground–wall reflection (bold solid curve) and the top reflection (bold dashed curve). The last case corresponds only to the top reflection of the building.

The ESPRIT algorithm is applied to the polarimetric interferometric SAR dataset over the area given by the mask of Fig. 3. A profile is extracted from the result to analyze the ESPRIT phase behavior, shown in Fig. 5. This profile is composed of two trees (A and B) and a building (C), located in the group of buildings (2) in Fig. 1. The ESPRIT algorithm gives two optimized interferometric phases ϕ_{opt_1} and ϕ_{opt_2}, one for each dominant scattering mechanism. Both phase behaviors discussed in the previous part are present in this profile: over (A) and (B) the difference between ϕ_{opt_1} and ϕ_{opt_2} is high, suggesting vegetation. Over (C), on the other hand, the ESPRIT interferometric phase behavior follows the principle illustrated in Fig. 4 (right), indicating the presence of a building.

It is possible to refine the building localization by analyzing, manually, the ESPRIT interferometric phases over areas given by the mask of Fig. 3 in order to generate a new mask, presented in Fig. 6. This mask contains only buildings; other media have been removed using the ESPRIT approach. This applies especially in the case for the vegetated areas (V) in comparison with Fig. 3.

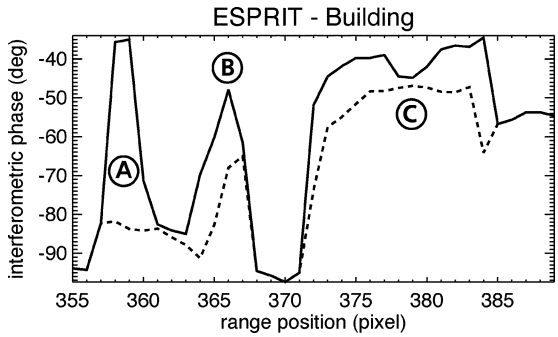

Fig. 5. Profile of the ESPRIT optimized interferometric phase. (Dashed line) ϕ_{opt_2}. (Solid line) ϕ_{opt_1}. The phase behavior is apparent: over A and B, there is a vegetation-type behavior as in Fig. 4 (left). Over C, the phase behavior corresponds to that of a building, as in Fig. 4 (right).

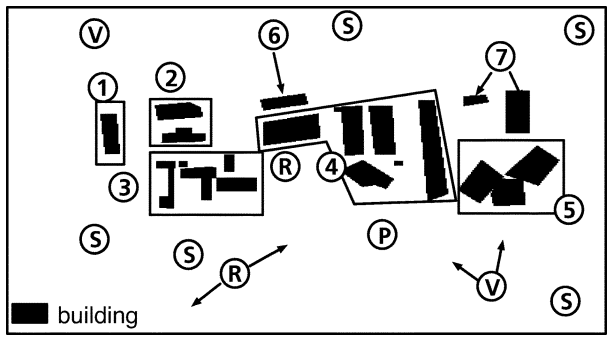

Fig. 6. New mask of building locations, obtained manually from Fig. 3, after an analysis of the interferometric phase given by the ESPRIT algorithm. Buildings are detected well, and vegetation areas are removed, as in the case of group (V).

D. Building Height Retrieval

The last step of the proposed method is the estimation of building heights. Over the areas given by the mask of Fig. 6, it is sufficient to convert the phase into height information using the following relation:

$$\Delta h(r) = \frac{\lambda}{4\pi} \frac{R(r)\sin\theta(r)}{B_\perp(r)} \phi_E(r) \tag{8}$$

where λ represents the wavelength, $R(r)$ is the range distance between the target and the master sensor at the range position (r), $\theta(r)$ is the look angle at the range position (r), $B_\perp(r)$ is the normal baseline, and $\phi_E(r)$ denotes the ESPRIT interferometric phase corresponding to the top of building. This formula gives a height difference between the real height and the reference height to which data are processed. In the case of airborne SAR data, each parameter has to be calculated for each range position. The heights of the buildings in the new mask of Fig. 6 are calculated using (8). From this, a three-dimensional (3-D) model of building groups (1)–(7) has been generated by calculating the average height in each building (in the mask of Fig. 6). The resulting model is shown in Fig. 7.

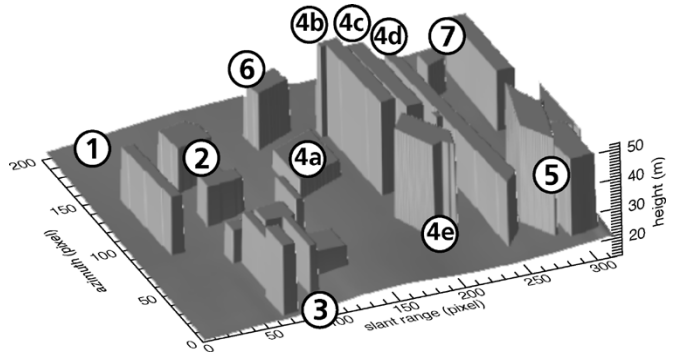

Fig. 7. Three-dimensional representation of building groups (1)–(7). This 3-D representation is obtained by calculating the average height in each building in the mask of Fig. 6.

TABLE I
COMPARISON BETWEEN THE VISUAL ESTIMATES AND THE HEIGHTS RETRIEVED BY THE PROPOSED APPROACH

building	1	2	4a	4b	4c	4d	4e
estimated (m)	18	13	5	30	26	18	29
visual estimation (m)	20	10	8	30	30	20	30

In the frame of this study, no precise ground truth including the number of buildings and building heights was available. Only a visual height estimation has been performed. By comparison with the aerial photography, more than 80% of buildings have been identified.

Table I is a comparison of the visual height estimates and the height estimates obtained using the proposed approach. There is a good agreement between the heights estimated from the ESPRIT interferometric phases and the visual ones. Apart from errors in the visual estimations, a significant source in this case is the small baseline, which implies a very high height ambiguity. This means that a small variation in phase can lead to large height differences. Nevertheless, this approach makes it possible to compute a relatively precise 3-D model of buildings.

III. CONCLUSION

This letter presents a method for building identification and height estimation based on polarimetric interferometric tools. Building identification is performed using a polarimetric classification procedure enhanced by the inclusion of interferometric information. The accuracy of building detection is improved by analyzing the optimized interferometric phase obtained with the ESPRIT algorithm. It becomes possible to distinguish two behaviors; one for vegetation, and one for buildings. After the buildings are located, a phase-to-height conversion is applied, taking into account the range dependencies in airborne SAR data, in order to estimate the height of building. From this, a 3-D representation of buildings can be obtained.

The detection and characterization of buildings using L-band SAR data is a very complex task. The proposed approach makes it possible to retrieve more than 80% of buildings with an acceptable height estimation, using L-band fully polarimetric SAR data, in repeat-pass acquisition mode. The spatial resolution is a limiting factor, and smaller buildings cannot be properly identified with the data used. Nevertheless, the proposed approach can be used to obtain useful results in urban areas, especially over areas with dense mixture of buildings and vegetation. In the future, building edges would have to be detected in order to completely characterize building using L-band fully polarimetric SAR data.

ACKNOWLEDGMENT

The authors wish to thank the German Aerospace Center for supplying the E-SAR data.

REFERENCES

[1] S. Guillaso, L. Ferro-Famil, A. Reigber, and E. Pottier, "Polarimetric interferometric SAR data analysis based on ESPRIT/MUSIC methods," presented at the *POLINSAR'03*, Frascati, Italy, Jan. 2003.

[2] S. R. Cloude and K. P. Papathanassiou, "Polarimetric SAR interferometry," *IEEE Trans. Geosci. Remote Sens.*, vol. 36, no. 5, pp. 1551–1565, Sep. 1998.

[3] J. S. Lee, M. R. Grunes, T. L. Ainsworth, L.-J. Du, D. L. Schuler, and S. R. Cloude, " Unsupervised classification using polarimetric decomposition and the complex Wishart classifier," *IEEE Trans. Geosci. Remote Sens.*, vol. 37, no. 5, pp. 2249–2258, Sep. 1999.

[4] S. R. Cloude and E. Pottier, "An entropy based classification scheme for land applications of polarimetric SAR," *IEEE Trans. Geosci. Remote Sens.*, vol. 35, no. 1, pp. 68–78, Jan. 1997.

[5] L. Ferro-Famil, E. Pottier, and J. S. Lee, "Unsupervised classification of multifrequency and fully polarimetric SAR images based on the H/A/Alpha—Wishart classifier," *IEEE Trans. Geosci. Remote Sens.*, vol. 39, no. 11, pp. 2332–2342, Oct. 2001.

[6] E. Pottier and J. S. Lee, "Unsupervised classification scheme of POLSAR images based on the complex wishart distribution and the $\ll H/A/\alpha \gg$ polarimetric decomposition theorem," presented at the *EUSAR'00*, Munich, Germany, May 2000.

[7] L. Ferro-Famil, E. Pottier, and J. S. Lee, *Unsupervised Classification of Natural Scenes from Polarimetric Interferometric SAR Data*. ser. Frontiers of Remote Sensing Information Processing, C. H. Chen, Ed. Dartmouth: Univ. Massachusetts, 2003.

[8] J. R. Huynen, "Phenomenological theory of radar targets," Ph.D. dissertation, Drukkerij, Bronder-Offset N. V., Rotterdam, The Netherlands, 1970.

[9] R. Roy and T. Kailath, "ESPRIT—Estimation of Signal Parameters via Rotational Invariance Technique," *IEEE Trans. Acoust., Speech, Signal Process.*, vol. 37, no. 7, pp. 984–995, Jul. 1989.

[10] H. Yamada, Y. Yamagushi, Y. Kim, E. Rodriguez, and W. M. Boerner, "Polarimetric SAR Interferometry for Forest Analysis Based on the ESPRIT Algorithm," *IEICE Trans. Electron.*, vol. E84-C, pp. 1917–1924, 2001.

[11] S. Guillaso, L. Ferro-Famil, A. Reigber, and E. Pottier, "Analyses of built-up area from polarimetric interferometric SAR images," presented at the *Proc. IGARSS*, Toulouse, France, Jul. 2003.

[12] ——, "Urban area analysis based on ESPRIT/MUSIC method using polarimetric interferometric SAR," presented at the *Proc. URBAN'03*, Berlin, Germany, May 2003.